Energy cascades in rapidly rotating and stratified turbulence within elongated domains

Adrian van Kan[1]†, and Alexandros Alexakis [1]

Laboratoire de Physique de l'Ecole normale supérieure, ENS, Université PSL, CNRS, Sorbonne Université, Université de Paris, F-75005 Paris, France

(Received xx; revised xx; accepted xx)

We study forced, rapildy rotating and stably stratified turbulence in an elongated domain using an asymptotic expansion at simultaneously low Rossby number $Ro \ll 1$ and large domain height compared to the energy injection scale, $h = H/\ell_{in} \gg 1$. The resulting equations depend on the parameter $\lambda = (hRo)^{-1}$ and the Froude number Fr. An extensive set of direct numerical simulations (DNS) is performed to explore the parameter space (λ, Fr). We show that a forward energy cascade occurs in one region of this space, and a split energy cascade outside it. At weak stratification (large Fr), an inverse cascade is observed for sufficiently large λ. At strong stratification (small Fr) the flow becomes approximately hydrostatic and an inverse cascade is always observed. For both weak and strong stratification, we present theoretical arguments supporting the observed energy cascade phenomenology. Our results shed light on an asymptotic region in the phase diagram of rotating and stratified turbulence, which is difficult to attain by brute-force DNS.

Key words:

1. Introduction

Rotating and stratified flows abound in the universe, from distant planets and stars to Earth's atmosphere and oceans (Salmon 1998; Pedlosky 2013; Vallis 2017), motivating a large number of theoretical and experimental studies in the past (Trustrum 1964; Maxworthy & Browand 1975; Gibson 1991; Davidson 2013). Typically these flows are turbulent, since they are characterised by large values of the Reynolds number Re, defined as the ratio of inertial forces to viscous forces. Also, the Péclet number Pe, given by the advective rate of change of temperature over the diffusive rate of change, is typically large. In a rotating system a Coriolis force arises, whose magnitude relative to the inertial force is measured by the Rossby number $Ro = \frac{U}{\Omega \ell}$, where U, ℓ are typical flow velocity and length scales, and Ω is the rotation rate. Density stratification and gravity give rise to buoyancy forces, whose strength relative to inertial forces is measured by the Froude number $Fr = \frac{U}{N\ell}$, where N is the buoyancy frequency. For $Ro < \infty$ and/or $Fr < \infty$, the isotropy of three-dimensional (3-D) turbulence is broken, since the rotation axis and gravity impose a direction in space.

† Email address for correspondence: avankan@ens.fr

When Ω is large, i.e. in the limit $Ro \to 0$, rotation suppresses variations of the motion along the axis of rotation and thus makes the flow quasi-two-dimensional, an effect described by the Taylor-Proudman theorem (Hough 1897; Proudman 1916; Taylor 1917; Greenspan et al. 1968). Similarly, when N is large, vertical motions are suppressed, and quasi-horizontal layers, so-called "pancakes", are favoured (Herring & Métais 1989; Waite & Bartello 2004; Brethouwer et al. 2007). A review of rotating and stratified flows is given in (Pouquet et al. 2017).

Turbulent energy transfer strongly depends on the dimension of space. In homogeneous isotropic 3-D turbulence, energy injected at large scales is transferred, by non-linear interactions, to small scales in a direct energy cascade (Frisch 1995). In the two-dimensional (2-D) Navier-Stokes equations, both energy and enstrophy are inviscid invariants and this fact constrains the energy transfer to be from small to large scales in an inverse energy cascade (Boffetta & Ecke 2012). Anisotropic turbulence, such as rotating and stratified turbulence in a finite layer, combines features of the 2-D and 3-D cases. For example, for forced (non-rotating, uniform-density) turbulence in a thin layer, there is a critical value h_c of the parameter $h = H/\ell_{in}$, with layer height H and forcing scale ℓ_{in}. At $h < h_c$ the flow becomes quasi-2-D and an inverse energy cascade forms (Celani et al. 2010; Benavides & Alexakis 2017; Musacchio & Boffetta 2017). In this state, part of the injected energy is transferred to larger scales and another part to smaller scales, forming a so-called *bidirectional* or *split* cascade (Alexakis & Biferale 2018). If the layer has a finite horizontal extent, in the absence of a large-scale damping mechanism, the inverse energy transfer leads to the formation of a condensate, where most of the energy is concentrated at the largest available scale (van Kan & Alexakis 2019; Musacchio & Boffetta 2019; van Kan et al. 2019). Similar transitions from a forward to an inverse cascade and to quasi-2-D motion have also been observed in other systems like magneto-hydrodynamic turbulence (Alexakis 2011; Seshasayanan et al. 2014; Seshasayanan & Alexakis 2016) and helically constrained flows (Sahoo & Biferale 2015; Sahoo et al. 2017) among others (see the articles by Alexakis & Biferale (2018) and Pouquet et al. (2019) for recent reviews).

Forced rotating turbulence in fluids of homogeneous density within a layer of finite height displays a similar transition when Ro is decreased below a threshold Ro_c, giving rise to a split cascade and quasi-2-D flow. The transition to a bidirectional cascade has been studied systematically by (Smith et al. 1996; Deusebio et al. 2014; Pestana & Hickel 2019), while the transition to a condensate regime was investigated by (Alexakis 2015; Yokoyama & Takaoka 2017; Seshasayanan & Alexakis 2018). Recently, (van Kan & Alexakis 2020) provided evidence that in the limit of simultaneously small Ro and large $h = H/\ell_{in}$, the transition to a bidirectional cascade occurs at a critical value of the parameter $\lambda = (hRo)^{-1} = \lambda_c \approx 0.03$. That study used direct numerical simulations (DNS) of an asymptotically reduced set of equations derived from the rotating Navier-Stokes equations to achieve extreme parameter regimes that are difficult to reach using a brute-force approach. In the present paper, we extend the results of (van Kan & Alexakis 2020) to the case of rotating and stably stratified flow.

For purely stratified flows, (Sozza et al. 2015) provided numerical evidence showing that there is a threshold height H_c, below which a split energy cascade appears, with $H_c \propto 1/N$ for $Fr \ll 1$ and $H \ll \ell_{in}$. In the case of combined rotating and stratified turbulence, there are numerous investigations reporting the observation of a split energy cascade (Smith & Waleffe 2002; Kurien et al. 2008; Marino et al. 2013, 2014; Rosenberg et al. 2015; Marino et al. 2015; Oks et al. 2017; Thomas & Daniel 2021). For unstable stratification in the presence of rotation, an inverse cascade has been reported, which leads to the formation of large-scale condensates (Favier et al. 2014; Guervilly et al. 2014; Rubio et al. 2014; Guervilly & Hughes 2017; Julien et al. 2018). Based on DNS at fixed layer height, (Marino et al. 2015) argued

that the ratio between the inverse energy flux to ϵ_- and the direct energy flux ϵ_+ is given by $\epsilon_-/\epsilon_+ \propto (RoFr)^{-1}$. However, they were only able to cover a limited parameter range and the possibility that the transition is critical as a function of $RoFr$ cannot be excluded (Alexakis & Biferale 2018). In general, one can say that the phase diagram of rotating stratified turbulence is far from understood. Such a phase diagram is particularly hard to obtain since it implies coverage of the 3-D parameter space (h, Ro, Fr). For instance, it is unknown whether there exists a critical surface separating a bidirectional and forward cascades in this space. To make progress, it is thus worth looking at particular limits.

Here, we focus on the asymptotic regime of deep layers $h \to \infty$ and fast rotation $Ro \to 0$, with $hRo = const. \equiv \lambda^{-1}$, and $Fr = O(1)$. We rely on an asymptotic expansion, similar to that used by van Kan & Alexakis (2020), which reduces the problem to a 2-D parameter space (λ, Fr). For $Fr \to \infty$, the problem further simplifies to the purely rotating case studied in (van Kan & Alexakis 2020), for which the transition is critical. In the following, we explore the (λ, Fr) parameter space by means of an extensive set of DNS.

The remainder of this paper is organised as follows. In section 2, we discuss the theoretical underpinnings of this study, in section 3 we describe our numerical set-up, in section 4 we present our numerical results. Finally, in section 5 we discuss our findings and conclude.

2. Theoretical background

In this section we describe the theoretical foundation of our work.

2.1. *From the Boussinesq system to the reduced equations*

The starting point of our investigation is given by the Boussinesq equations in a frame of reference rotating at a constant rate $\mathbf{\Omega} = \Omega\hat{e}_\parallel$, for a linear background density profile $\rho(\mathbf{x}, t) = \rho_0 - \alpha(\mathbf{x} \cdot \hat{e}_\parallel) + \delta\rho(\mathbf{x}, t)$, with position $\mathbf{x}$, time t, background density $\rho_0 = cst.$, stratification strength $\alpha > 0$, and $|\rho - \rho_0| \ll \rho_0$. Gravity and stratification are taken to be parallel to the rotation axis. In their dimensional form, these equations read

$$\partial_t \mathbf{u} + \mathbf{u} \cdot \nabla\mathbf{u} + 2\Omega\hat{e}_\parallel \times \mathbf{u} = -\nabla p + N\phi\hat{e}_\parallel + \nu\nabla^2\mathbf{u} + \mathbf{f}, \tag{2.1}$$

$$\partial_t \phi + \mathbf{u} \cdot \nabla\phi = -Nu_\parallel + \kappa\nabla^2\phi, \tag{2.2}$$

$$\nabla \cdot \mathbf{u} = 0, \tag{2.3}$$

with velocity $\mathbf{u}$, pressure (divided by ρ_0) p, kinematic viscosity ν, forcing $\mathbf{f}$ (only acting on momentum), buoyancy frequency $N = \sqrt{g\alpha/\rho_0} = cst.$, rescaled density perturbation $\phi(\mathbf{x}, t) = N\delta\rho$, and diffusivity κ. The domain considered here is the cuboid of dimensions $2\pi L \times 2\pi L \times 2\pi H$, depicted in figure 1, with periodic boundary conditions. For any vector $\mathbf{F}$, we define the parallel and perpendicular components as $\mathbf{F}_\parallel = (\mathbf{F} \cdot \hat{e}_\parallel)\hat{e}_\parallel = F_\parallel\hat{e}_\parallel$, and $\mathbf{F}_\perp = \mathbf{F} - \mathbf{F}_\parallel$.

In the present study, we will explore the regime of simultaneously large h and small Ro with $Fr = O(1)$. Brute-force simulations at small Ro are costly, since very small time steps are required to resolve fast inertio-gravity waves. Instead, we exploit an asymptotic expansion based on the Boussinesq equations, first introduced in (Julien et al. 1998), which allows one to investigate the properties of the transition to a split cascade in an efficient manner. We consider a stochastic forcing, injecting energy at a constant mean rate into both perpendicular and parallel motions $\langle \mathbf{f}_\perp \cdot \mathbf{u}_\perp \rangle = \langle f_\parallel u_\parallel \rangle = \epsilon_{in}/2$, where $\langle \cdot \rangle$ denotes an ensemble average over infinitely many realisations of then noise. The forcing is chosen to be 2-D (independent of the parallel direction), for simplicity, and filtered in Fourier space to act only on a ring of perpendicular wavenumbers centered on $|\mathbf{k}| = k_f = 1/\ell_{in}$. A similar 2-D forcing has been widely used in previous studies on the transition toward an inverse cascade (Deusebio

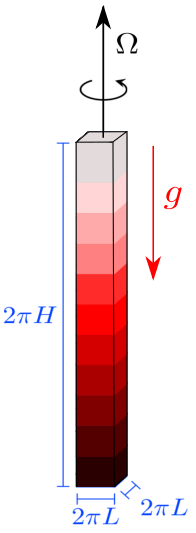

Figure 1: The long, rapidly rotating domain with stratification. The black arrow pointing upwards indicates the rotation axis, the red arrow pointing downwards indicates gravity.

et al. 2014; Smith et al. 1996; Celani et al. 2010; van Kan & Alexakis 2020). In general, the transition to an inverse cascade can depend on the choice of forcing. Recent work in thin-layer turbulence by Poujol et al. (2020) suggests that a 3-D forcing, which includes non-zero parallel wavenumbers, is less efficient at generating an inverse cascade and delays the onset.

The forcing imposes a length scale ℓ_{in}, as well as a time scale $\tau_{in} = (\ell_{in}^2/\epsilon_{in})^{1/3}$, and thus a velocity scale $(\epsilon_{in}\ell_{in})^{1/3}$. In terms of these scales, the Rossby number $Ro = (\tau_{in}\Omega)^{-1}$, and we adopt the ϕ scale $\ell_{in}N$. The typical scale of parallel variations is H, rather than ℓ_{in}. Nondimensionalising the equations with these scales, we consider the limit $h = H/\ell_{in} = 1/\epsilon$ with $0 < \epsilon \ll 1$ and $Ro = O(\epsilon)$, such that $\lambda = (hRo)^{-1} = O(1)$ is independent of ϵ. A multiple-scale expansion (Sprague et al. 2006) or a heuristic derivation, analogous to that presented in (van Kan & Alexakis 2020), can be used to obtain a set of asymptotically reduced equations for the parallel components of velocity $u_\parallel$ and vorticity $\omega_\parallel = (\nabla \times \mathbf{u}) \cdot \hat{e}_\parallel$, whose dimensionless form reads

$$\partial_t u_\parallel + \mathbf{u}_\perp \cdot \nabla_\perp u_\parallel = -2\lambda \partial_\parallel \nabla_\perp^{-2} \omega_\parallel - \frac{1}{Fr}\phi + \frac{1}{Re}\nabla_\perp^2 u_\parallel + f_\parallel, \tag{2.4}$$

$$\partial_t \omega_\parallel + \mathbf{u}_\perp \cdot \nabla_\perp \omega_\parallel = +2\lambda \partial_\parallel u_\parallel + \frac{1}{Re}\nabla_\perp^2 \omega_\parallel + f_\omega, \tag{2.5}$$

$$\partial_t \phi + \mathbf{u}_\perp \cdot \nabla_\perp \phi = \frac{1}{Fr} u_\parallel + \frac{1}{Pe}\nabla_\perp^2 \phi, \tag{2.6}$$

where $\partial_\parallel = \hat{e}_\parallel \cdot \nabla$, $\nabla_\perp = \nabla - \hat{e}_\parallel \partial_\parallel$, and the nondimensional parameters $Fr = (\epsilon_{in}/\ell_{in}^2)^{1/3}/N$, $\lambda = (hRo)^{-1} = \ell_{in}^{5/3}\Omega/(\epsilon_{in}^{1/3}H)$, $Re = (\epsilon_{in}\ell_{in}^4)^{1/3}/\nu$, $Pe = (\epsilon_{in}\ell_{in}^4)^{1/3}/\kappa$. The perpendicular velocity $\mathbf{u}_\perp$ is divergence-free to leading order, $\nabla_\perp \cdot \mathbf{u}_\perp = 0$, which permits us to write it in terms of a stream function ψ, such that $\mathbf{u}_\perp = \hat{e}_\parallel \times \nabla\psi$, and $\omega_\parallel = \nabla_\perp^2 \psi$. These nondimensional equations are valid in the rescaled domain $2\pi\Lambda \times 2\pi\Lambda \times 2\pi$, with $\Lambda = L/\ell_{in}$. Importantly, in eqs. (2.4) and (2.5), all the information about H, Ω is contained in the single parameter λ.

2.2. *Conservation laws*

For infinite Re and Pe, the system conserves the total energy $\mathcal{E} = \frac{1}{2}\int(\mathbf{u}^2 + \phi^2)d^3x$. In addition, the *potential vorticity*

$$q = 2\lambda\partial_z\phi - \omega_\parallel/Fr + (\partial_y u_\parallel)(\partial_x\phi) - (\partial_x u_\parallel)(\partial_y\phi) \tag{2.7}$$

(in Cartesian coordinates, with the parallel direction being z) is conserved along each fluid parcel trajectory. Eq. (2.7) is a simplified, Boussinesq version of Ertel's full potential vorticity (Ertel 1942) (the full form applies to compressible flow). The material conservation of q implies that $C_n = \int q^n d^3x$ is conserved for all n, where the special case $n = 2$ is known as *potential enstrophy*. In 2-D turbulence, energy and enstrophy are both quadratic functionals of the stream function, with enstrophy containing higher spatial derivatives. The simultaneous conservation of the two quantities constrains the energy cascade to be to larger scales, and the enstrophy to smaller scales. By contrast, C_2 is not directly related to the kinetic or potential energy, and does not imply a straightforward constraint for cascade directions, except in a special case, which shall be discussed later.

Eqs. (2.4), (2.5) and (2.6) are closely related to well-known models in geophysical fluid dynamics. Since the leading-order perpendicular velocity is in geostrophic balance, and only the perpendicular velocity appears in the advection terms, the model resembles the classical quasi-geostrophic equations valid in thin layers (Pedlosky 2013). Indeed (2.4-2.6) have been referred to as *generalised quasi-geostrophic* equations (Julien et al. 2006). Variants of the reduced equations have been applied in a variety of contexts, such as rotating turbulence (Nazarenko & Schekochihin 2011), rapidly rotating convection (Sprague et al. 2006; Grooms et al. 2010; Julien et al. 2012a,b; Rubio et al. 2014; Maffei et al. 2021), as well as dynamos driven by rapidly rotating convection (Calkins et al. 2015).

2.3. *Inertio-gravity waves and slow modes*

A fundamental property of rotating and stratified flows is that they support inertio-gravity waves. In the full Boussinesq equations (2.1-2.3), the dispersion relation of these waves reads

$$\sigma^2(\mathbf{k}) = \frac{4\Omega^2 k_\parallel^2 + N^2 k_\perp^2}{k^2}, \tag{2.8}$$

where σ is the wave frequeny, Ω is the rotation rate, N is the buoyancy frequency, $\mathbf{k}$ is the wave vector, $k_\parallel$ is the component of the wave vector along the rotation axis, $k_\perp$ the component perpendicular to the rotation axis, and $k^2 = k_\parallel^2 + k_\perp^2$. In the framework of the reduced equations of motion (2.4-2.6), this simplifies, in nondimensional form, to

$$\sigma^2(\mathbf{k}) = 4\lambda^2\frac{k_\parallel^2}{k_\perp^2} + \frac{1}{Fr^2}, \tag{2.9}$$

where σ and the wavenumber components are nondimensional. At large Ω, (2.8) implies high wave frequencies, requiring a small time step to be resolved numerically. In the reduced equations, all parameters are of order one, which makes numerical simuation more efficient.

The full set of linear modes of rotating stratified flow has been studied in great detail (Leith 1980; Bartello 1995; Sukhatme & Smith 2008; Herbert et al. 2014). Here we just summarise some relevant results. Formally, linearising (2.4-2.6), one obtains an equation of the form $\dot{\mathbf{Z}}(\mathbf{k}) = \mathbf{L}(\mathbf{k})\mathbf{Z}(\mathbf{k})$, with $\mathbf{Z}(\mathbf{k}) = (k_\perp\hat{\psi}(\mathbf{k}), \hat{u}_\parallel(\mathbf{k}), \hat{\phi}(\mathbf{k}))$ with hats denoting Fourier transforms, and a 3×3 matrix $\mathbf{L}$. The eigenvalues of $\mathbf{L}$ are $+\sigma(\mathbf{k}), -\sigma(\mathbf{k}), 0$, with $\sigma(\mathbf{k}) > 0$ given by eq. (2.9). Thus, in addition to waves with frequencies $\pm\sigma$, one also finds linear eigenmodes with zero frequency at every wavenumber. The corresponding normalised

eigenvector is

$$\mathbf{Z}_0(\mathbf{k}) = \frac{1}{\sigma(\mathbf{k})k_\perp}\left(-ik_\perp Fr^{-1},\ 0,\ 2\lambda k_\parallel\right), \tag{2.10}$$

which notably has a vanishing $\hat{u}_\parallel$ component. These *slow* modes with zero frequency span the so-called *slow manifold*. The normalised eigenvectors of $\mathbf{L}$ with eigenvalues $\pm\omega(\mathbf{k})$ are

$$\mathbf{Z}_\pm(\mathbf{k}) = \frac{1}{\sqrt{2}\sigma(\mathbf{k})k_\perp}\left(2\lambda k_\parallel,\ \pm\sigma(\mathbf{k})k_\perp,\ -ik_\perp Fr^{-1}\right). \tag{2.11}$$

which has a nonvanishing $\hat{u}_\parallel$ component. We highlight that the wave modes have zero potential vorticity at the linear level. The slow modes are thus the vortical modes of the flow.

In order for wave modes to interact efficiently with the slow modes, the inverse wave frequency of the slowest waves must be comparable to the eddy turnover time scale of the turbulent 2-D flow τ_{in}. In the purely rotating case ($Fr \to \infty$), this argument was successfully by van Kan & Alexakis (2020) to predict the dependence of the energy cascades on λ: forward cascade at $\lambda < \lambda_c \approx 0.03$ and inverse cascade at $\lambda > \lambda_c$. For the rotating and stratified case, two cases can be anticipated based on (2.9).

2.4. *Weak stratification: the passive-scalar limit*

At weak stratification ($Fr > 1$), the system is likely to be close to the purely rotating case, such that a transition should occur when $\lambda > \lambda_c(Fr)$. While we do not predict the dependence of $\lambda_c(Fr)$, it seems likely that $\lambda_c = (H_c Ro_c)^{-1}$ increases with stratification. This is because as the weak stratification is increased (while remaining weak), kinetic and potential energy become more strongly coupled, and more kinetic energy will be converted to potential energy, which behaves approximately like a passive scalar at weak stratification. For passive scalars, it is well known that scalar variance (potential energy) cascades forward (to small scales) (Warhaft 2000; Falkovich et al. 2001; Celani et al. 2004). Therefore stratification will counteract the inverse cascade. Thus it appears reasonable that faster rotation, i.e. higher λ, should be required at weak stratification for generating an inverse energy flux. A similar effect has been observed in thin-layer turbulence, where a decrease of the critical height has been observed with increased stratification (Sozza et al. 2015).

2.5. *Strong stratification: the hydrostatic limit*

For strong stratification ($Fr \ll 1$) and large λ, the dominant balance in (2.4) is given by

$$2\lambda\partial_\parallel\nabla_\perp^{-2}\omega_\parallel = -\phi/Fr. \tag{2.12}$$

Eq. (2.12) is a form of hydrostatic balance, which is common in geophysical flows (Vallis 2017). To see this, one can identify the stream function of the perpendicular flow as $\nabla_\perp^{-2}\omega_\parallel = \psi$, which follows from $\mathbf{u}_\perp = \hat{e}_\parallel \times \nabla\psi$. Comparing the latter relation to geostrophic balance, between Coriolis force and perpendicular pressure gradient, one further deduces that ψ is proportional to the pressure. Hence eq. (2.12) is a balance between the vertical (parallel) pressure gradient and gravity, i.e. hydrostatic balance.

We note that modes in the slow manifold defined in section 2.3 correspond to balanced motion in the sense that they satisfy (2.12) at the linear level. At the nonlinear level though, even if the flow starts at hydrostatic balance its nonlinear evolution can disrupt it. However, in the limit of high wave frequencies one can expect that the inertio-gravity waves will decouple from the slow manifold, which will therefore evolve independently, always satisfying eq. (2.12). Such a limit can be formally captured by letting $\lambda \to \lambda/\epsilon, Fr^{-1} \to Fr^{-1}/\epsilon, u_\parallel \to \epsilon u_\parallel$, with $\epsilon \ll 1$, while $\omega_\parallel, \phi \to \omega_\parallel, \phi$. In this limit $\omega_\parallel$ and ϕ evolve according to (2.5) and (2.6), with $u_\parallel$ acting as a Lagrange multiplier, imposing eq. (2.12) (in a similar way as pressure

imposes incompressibility in 3D Navier Stokes). Equations (2.5), (2.6), and (2.16) thus constitute a dynamic hydrostatically balanced system. Note that for $\lambda \gg Fr^{-1}$ the dynamic hydrostatic balance just corresponds to a two-dimensionalization of the flow. This is because hydrostatic balance implies small $\partial_\parallel \psi$ in this limit, and the omega equation constrains $u_\parallel$ to be small, such that that the flow is approximately two-dimensional with two components. However, when Fr is of order one or smaller the flow is not necessarily 2-D. For small or $O(1)$ values of λ, the dynamic hydrostatic balance limit is expected to hold when the wave frequency is much larger than typical eddy turn over time, i.e. $Fr \ll 1$. We highlight the fact that the combination $\lambda Fr \propto Fr/Ro \propto \Omega/N$, which has been indentified as a control parameter in previous studies (Smith & Waleffe 2002; Marino et al. 2015), appears naturally here in eq. (2.12).

If (2.12) holds at every time step, then the stream function and ϕ fields are directly related. This implies that, at leading order, eq. (2.7) becomes

$$q = -Fr^{-1}\left[(2\lambda Fr)^2\partial_\parallel^2 + \nabla_\perp^2\right]\psi + O(\epsilon) \equiv -Fr^{-1}\overline{\nabla}^2\psi + O(\epsilon), \tag{2.13}$$

where we identified the rescaled Laplace operator $\overline{\nabla}^2 \equiv (2\lambda Fr)^2\partial_\parallel^2 + \nabla_\perp^2$. The potential enstrophy takes the leading-order form

$$C_2 = Fr^{-2}\int\left(\overline{\nabla}^2\psi\right)^2 d^3x + O(\epsilon) \tag{2.14}$$

while the total energy becomes, at leading order,

$$\mathcal{E} = \frac{1}{2}\int\left(\overline{\nabla}\psi\right)^2 + O(\epsilon^2). \tag{2.15}$$

Both energy and potential enstrophy are expressed entirely in terms of ψ, with the potential enstrophy containing higher-order spatial derivatives. This allows one to make an argument analogous to that put forward by (Fjørtoft 1953) for 2-D turbulence: if $\mathcal{E}$ and C_2 are initially injected at a scale ℓ_{in} and subsequently spread out over different length scales by nonlinear interactions, then it can simply be shown in Fourier space that most of the energy must be transferred to scales larger than ℓ_{in}, and potential enstrophy to scales smaller than ℓ_{in}, in order for the conservation laws to be satisfied (see section 3.5 of (Alexakis & Biferale 2018)). The direct link between the density perturbation field and the stream function given by hydrostatic balance implies that both potential and perpendicular kinetic energy cascade inversely.

We note that taking the time derivative of (2.12) gives the intriguing diagnostic (as opposed to prognostic) relation

$$\overline{\nabla}^2 u_\parallel = S, \tag{2.16}$$

with the source term

$$S = Fr^2\left\{Fr^{-1}\nabla_\perp^2[(\mathbf{u}_\perp\cdot\nabla_\perp)\phi] + 2\lambda\partial_\parallel[(\mathbf{u}_\perp\cdot\nabla_\perp)\omega_\parallel]\right\}. \tag{2.17}$$

Equation (2.16) is a variant of the *omega equation*, which is well known (for an arbitrary stable background density profile) in meteorology (Hoskins et al. 1978, 2003). In the meteorological literature, pressure is often taken as the vertical coordinate in an ideal-gas atmosphere. In this coordinate system, the vertical velocity is conventionally denoted by ω by meteorologists, hence the name of the equation. The omega equation has been used extensively for diagnosing vertical velocities, which are highly relevant for weather phenomena, from observed vorticity and temperature fields.

3. Numerical set-up and methodology

In this section, we describe the numerical set-up used in the present study. The partial differential equations that we solve numerically in a domain $2\pi\Lambda \times 2\pi\Lambda \times 2\pi$ are given by (2.4), (2.5) and (2.6) with modified dissipative terms

$$\partial_t u_\parallel + \mathbf{u}_\perp \cdot \nabla_\perp u_\parallel + 2\lambda\partial_\parallel \nabla_\perp^{-2}\omega_\parallel = -\frac{\phi}{Fr} - \frac{(-\nabla_\perp^2)^n u_\parallel}{Re_\perp} - \frac{(-\partial_\parallel^2)^m u_\parallel}{Re_\parallel} + f_\parallel, \tag{3.1}$$

$$\partial_t \omega_\parallel + \mathbf{u}_\perp \cdot \nabla \omega_\parallel - 2\lambda\partial_\parallel u_\parallel = - \frac{(-\nabla_\perp^2)^n \omega_\parallel}{Re_\perp} - \frac{(-\partial_\parallel^2)^m \omega_\parallel}{Re_\parallel} + f_\omega, \tag{3.2}$$

$$\partial_t \phi + \mathbf{u}_\perp \cdot \nabla \phi = +\frac{u_\parallel}{Fr} - \frac{(-\nabla_\perp^2)^{n_\phi} \phi}{Pe_\perp} - \frac{(-\partial_\parallel^2)^{m_\phi} \phi}{Pe_\parallel}. \tag{3.3}$$

Note that there is no large-scale friction term, such that an inverse cascade can develop unhindered and accumulate energy the scale of the box. Moreover, the density perturbation field ϕ is not forced directly in our simulations. As in (van Kan & Alexakis 2020), the parallel dissipation terms, which do not appear in (2.4), (2.5) and (2.6), are added for numerical reasons, suppressing the formation of exceedingly large parallel wavenumbers. We choose the hyperviscosity exponents $n = m = n_\phi = m_\phi = 4$ for all simulations.

Equations (3.1-3.3) are controlled by seven nondimensional parameters. In addition to Λ, λ and Fr, which are defined identically to eq. (2.4-2.6), there are two Reynolds numbers and two Peclet numbers associated with perpendicular and parallel diffusion terms, respectively:

$$Re_\perp = \frac{\epsilon_{in}^{1/3}\ell_{in}^{2n-2/3}}{\nu_n},\ Re_\perp = \frac{\epsilon_{in}^{1/3}\ell_{in}^{2m-2/3}}{\nu_m},\ Pe_\perp = \frac{\epsilon_{in}^{1/3}\ell_{in}^{2n_\phi-2/3}}{\kappa_n},\ Pe_\parallel = \frac{\epsilon_{in}^{1/3}\ell_{in}^{2m_\phi-2/3}}{\kappa_{m_\phi}} \tag{3.4}$$

with hyperviscosities ν_n, ν_m and hyperdiffusivities $\kappa_{n_\phi}, \kappa_{m_\phi}$.

We solve equations (3.1-3.3) in the triply periodic domain using a speudo-spectral code based on the Geophysical High-order Suite for Turbulence, including 2/3-aliasing (see Mininni et al. (2011)). A total of 71 runs were performed at a resolution of 512^3 with $\Lambda = 32$, of which 63 runs at $Re_\perp = Re_\parallel = Pe_\perp = Pe_\perp\| = 9.2 \times 10^3$, for different values of Fr and λ, and an additional 8 runs with $Re_\parallel$ and $Pe_\parallel$ halved, and $Re_\perp, Pe_\perp$ unchanged to verify that our results do not depend on the parallel dissipation terms added for numerical reasons.

In order to characterise the energy cascades, we measure several quantities in every run, which are defined below, with hats indicating Fourier transforms. The 2-D kinetic energy spectrum is defined as

$$E_{kin}(k_\perp, k_\parallel) = \frac{1}{2} \sum_{k_\perp - \frac{1}{2} \leqslant p_\perp < k_\perp + \frac{1}{2}} \left(\frac{|\hat{\omega}_\parallel(\mathbf{p}_\perp, k_\parallel)|^2}{k_\perp^2} + |\hat{u}_\parallel^2(\mathbf{p}_\perp, k_\parallel)|^2 \right), \tag{3.5}$$

and the 2-D potential energy spectrum as

$$E_{pot}(k_\perp, k_\parallel) = \frac{1}{2} \sum_{k_\perp - \frac{1}{2} \leqslant p_\perp < k_\perp + \frac{1}{2}} |\hat{\phi}(\mathbf{p}_\perp, k_\parallel)|^2, \tag{3.6}$$

where hats denote Fourier transforms. The one-dimensional (1-D) energy spectrum is

obtained by summing the 2-D spectra over $k_\parallel$,

$$E_{kin}(k_\perp) = \sum_{k_\parallel} E_{kin}(k_\perp, k_\parallel) \equiv E^{\perp}_{kin}(k_\perp) + E^{\parallel}_{kin}(k_\perp), \tag{3.7}$$

$$E_{pot}(k_\perp) = \sum_{k_\parallel} E_{pot}(k_\perp, k_\parallel), \tag{3.8}$$

where $E^{\perp}_{kin}$ contains all terms involving $\hat{\omega}_\parallel$ and $E^{\parallel}_{kin}$ contains all terms involving $\hat{u}_\parallel$. In addition, we define the total energy spectrum $E_{tot} = E_{kin} + E_{pot}$.

The 2-D dissipation spectra are defined as

$$D_{kin}(k_\perp, k_\parallel) = \sum_{k_\perp - \frac{1}{2} \leqslant p_\perp < k_\perp + \frac{1}{2}} (\nu_n p_\perp^{2n} + \nu_m k_\parallel^{2m}) \left(\frac{|\hat{\omega}_\parallel(\mathbf{p}_\perp, k_\parallel)|^2}{k_\perp^2} + |\hat{u}^2_\parallel(\mathbf{p}_\perp, k_\parallel)|^2 \right), \tag{3.9}$$

$$D_{pot}(k_\perp, k_\parallel) = \sum_{k_\perp - \frac{1}{2} \leqslant p_\perp < k_\perp + \frac{1}{2}} (\kappa_{n_\phi} p_\perp^{2n_\phi} + \kappa_{m_\phi} k_\parallel^{2m_\phi}) |\hat{\phi}(\mathbf{p}_\perp, k_\parallel)|^2, \tag{3.10}$$

giving the total dissipation spectrum $D_{tot} = D_{kin} + D_{pot}$. Finally, the spectral energy fluxes in the perpendicular direction through a cylinder of radius $k_\perp$ in Fourier space are defined as

$$\Pi^{\perp}_{kin}(k_\perp) = \langle (u_\perp)^{<}_{k_\perp} \cdot [(\mathbf{u}_\perp \cdot \nabla_\perp)\mathbf{u}_\perp] \rangle, \tag{3.11}$$

$$\Pi^{\parallel}_{kin}(k_\perp) = \langle (u_\parallel)^{<}_{k_\perp} [(\mathbf{u}_\perp \cdot \nabla_\perp) u_\parallel] \rangle, \tag{3.12}$$

$$\Pi_{pot}(k_\perp) = \langle \phi^{<}_{k_\perp} [(\mathbf{u}_\perp \cdot \nabla_\perp)\phi] \rangle, \tag{3.13}$$

with the total energy flux defined as $\Pi_{tot} \equiv \Pi^{\perp}_{kin} + \Pi^{\parallel}_{kin} + \Pi_{pot}$, where for any field A,

$$A^{<}_{k_\perp}(\mathbf{x}) \equiv \sum_{\substack{\mathbf{p} \\ p_\perp < k_\perp}} \hat{A}(\mathbf{p}) \exp(i\mathbf{p} \cdot \mathbf{x}). \tag{3.14}$$

Every run is initialised at a random small-energy configuration, and continued until

1. an inverse energy flux is observed, with kinetic energy piling up at the large scales,
2. or a purely forward cascade is observed and the system has reached steady state.

4. Simulation results

In this section we present the results of our simulations.

4.1. *Overview of parameter space*

First we provide an overview of the runs. Figure 2 shows a regime diagram indicating for which values of λ and Fr an inverse cascade in kinetic energy was observed. Two regions can be discerned: a finite region (red diamonds) near the origin in terms of (λ, Fr^{-1}), where a forward cascading state is observed, and a surrounding region (blue circles) at larger λ (faster rotation / shallower box) and larger Fr^{-1} (strong stratification), where an inverse energy cascade arises. The boundary between the two is tentatively shown by the dashed line. The boundary between the two regions is consistent with our expectations from section 2: first, for $Fr > 1$ (weaker stratification), there is a (roughly linear) increase in λ_c, i.e. the critical $(Roh)^{-1}$, with Fr^{-1}. While we do not offer a theoretical prediction for the linear scaling, an identical scaling $h_c \propto 1/N$ has been suggested for strongly stratified turbulence in a thin layer (Sozza et al. 2015). Second, when Fr is lowered beyond $Fr \approx 1$, the system enters the hydrostatic regime, and a direct energy cascade turns into an inverse cascade.

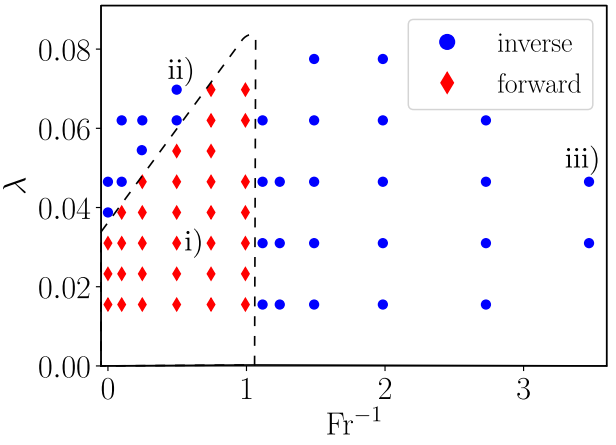

Figure 2: Regime diagram showing the direction of the kinetic energy cascade for various values of the parameters (λ, Fr^{-1}). A tentative boundary between forward and split cascading states is shown by the dahsed line. The labels i), ii) and iii) indicate the three states to be examined in more detail below.

4.2. *Spectra*

In the following, we illustrate three different representative cases highlighted in figure 2,

i) $\lambda = 0.03$ $Fr^{-1} = 0.5$ (no inverse cascade),
ii) $\lambda = 0.07$, $Fr^{-1} = 0.5$ (weak stratification, inverse cascade),
iii) $\lambda = 0.045$, $Fr^{-1} = 3.5$ (strong stratification, inverse cascade).

The 1-D energy spectra are shown in figure 3. For case i), in the forward-cascading regime, there is a spectral maximum in both perpendicular and parallel kinetic energy at $k_\perp \approx k_f/2$. A similar phenomenon is reported in (van Kan & Alexakis 2020) for the purely rotating case, where an instability mechanism was suggested as the cause for this secondary maximum. The potential energy spectrum is peaked at yet larger scales $k_\perp < k_f/2$. While we do not offer a theoretical explanation for the local spectral maxima at scales larger than the forcing scale, the similarity with the phenomenology of the rotating case suggests that a related instability mechanism may be at play. The potential energy spectrum is comparable to the parallel kinetic energy spectrum, except at the largest scales, where it is comparable to the perpendicular kinetic energy, and at the forcing scale, where it is smaller, since potential energy is not directly forced. For case ii), where an inverse cascade is present at weak stratification, the perpendicular kinetic energy spectrum shows a maximum at the largest scale $k_\perp = 1$, where it dominates the total energy. The parallel kinetic energy and and the potential energy, by contrast, do not show a maximum at the largest scales. Finally, in case iii), where an inverse cascade is present at strong stratification, both the perpendicular kinetic energy spectrum and the potential energy spectrum shows maximum at $k_\perp = 1$, with a clear power-law range at $k_\perp < k_f$. The shape of the potential energy spectrum is strikingly similar to the perpendicular kinetic energy, only differing by constant factor of around 0.3 over two decades in $k_\perp$. One also observes a peak at the forcing scale, although the potential energy is not directly forced. These observations indicate that the density field and the parallel vorticity are non-trivially related to each other for all scales but the very smallest. As discussed in section 2, this can occur as the consequence of hydrostatic balance. This will be examined in section 4.5. In case iii), the parallel kinetic energy does not show a secondary maximum.

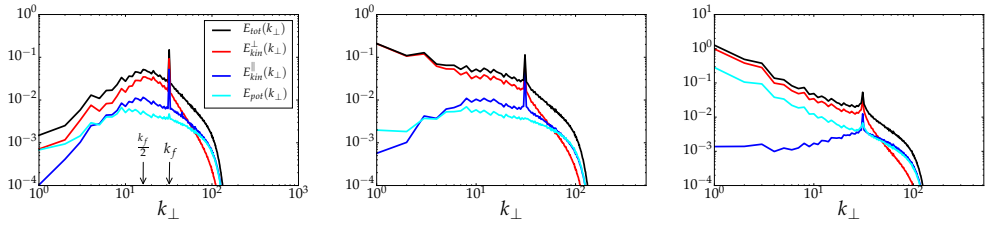

Figure 3: Double logarithmic plots of the contributions to the 1-D energy spectra according to equations (3.7) and (3.8). Left: case i), center: case ii), right: case iii). The legend on the left applies to all panels.

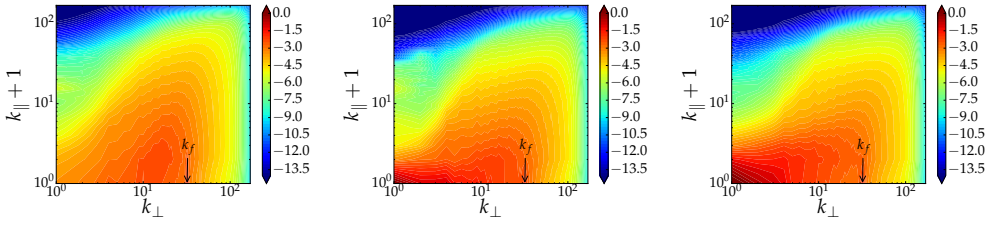

Figure 4: Filled contour plots of the 2-D kinetic energy spectrum $E_{kin}(k_\perp, k_\parallel)$ defined in equation (3.5), as a function of $k_\perp$, $k_\parallel$ for cases i) to iii) (left to right).

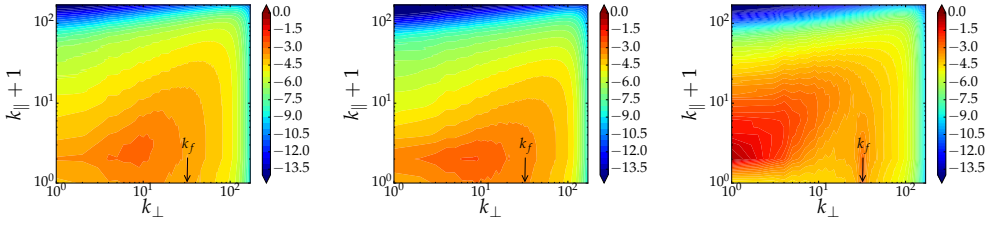

Figure 5: Filled contour plots of 2-D potential energy spectrum $E_{pot}(k_\perp, k_\parallel)$ defined in (3.6) versus $k_\perp$, $k_\parallel$ for cases i) to iii) (left to right).

The 2-D kinetic energy spectra (sum of perpendicular and parallel contributions) are shown in figure 4. In case i), the spectral maximum at $k_\perp \approx k_f/2$ is seen to extend to $k_\parallel > 0$. In cases ii) and iii), the spectral maximum at $k_\perp = 1$ is seen to stem primarily from contributions at $k_\parallel = 0$. The 2-D potential energy spectrum is shown figure 5. For cases i) and ii), there is a maximum at intermediate $k_\perp$, with $k_\parallel = 1$. By contrast, for case iii) there is a clear build-up of potential energy at $k_\perp = 1$, and maximum at $k_\parallel = 1$ (and some contributions from $k_\parallel = 2$). In case iii), there is only little potential energy at $k_\parallel = 0$, even though the kinetic energy spectrum peaks at $k_\parallel = 0$, which is compatible with hydrostatic balance (2.12).

4.3. *Energy fluxes*

Figure 6 shows the different components of the energy flux (normalised by the injection rate) for the three cases. In case i), the total flux vanishes at $k_\perp < k_f$, while it is positive at $k_\perp > k_f$. At $k_\perp > k_f$, the flux of perpendicular kinetic energy is close to zero, and negligible compared to the large forward (positive) fluxes of parallel kinetic energy and potential energy. At the largest scales, all fluxes vanish, i.e. no energy is transferred to or

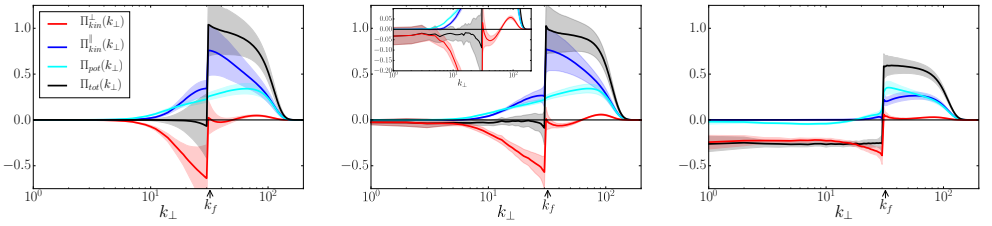

Figure 6: Average energy fluxes (non-dimensionalised by the injection rate ϵ) for cases i (left), ii (center) and iii) right. The shaded area around curves shows one standard deviation of fluctuations about the average. In the central panel, the inset shows a zoom on negative-flux range.

from the large scales by nonlinear interactions. For intermediate scales between $k_\perp = k_f$ and $k_\perp \approx 5$, there is a wavenumber range over which there is a flux loop leading to zero net flux: the flux of pependicular kinetic energy is negative, i.e. inverse, while the kinetic energy in the parallel components of velocity and the potential energy show a positive (i.e. forward) flux, with the sum of the three cancelling out. In case ii), the flux loop persists at these intermediate scales, but the net flux is slightly negative (inverse), rather than zero. This inverse flux, which amounts to about 3% of the energy injection rate, reaches all the way to the largest scales $k_\perp = 1$, as the inset in figure 6 shows. The parallel kinetic energy and potential energy fluxes are very similar to case i), being positive definite everywhere. In case iii), there is a strong net inverse flux, making up around 30% of energy injection rate. Remarkably, while the dominant contribution to this inverse flux stems from the perpendicular kinetic energy, there is also an inverse flux of potential energy. In cases i) and ii), by constrast, the potential energy flux is positive definite. The strong stratification in case iii) breaks the passive-scalar-like evolution of the the potential energy mentioned in section 2, which otherwise constrains the potential energy to cascade to small scales only. Moreover, the fact that both perpendicular kinetic energy and potential energy cascade inversely is compatible with the ϕ and $\omega_\parallel$ fields being linked by hydrostatic balance, which is shown to be the case in section 4.5.

4.4. *Well-resolvedness*

For each run, we verify well-resolvedness by inspecting the total dissipation spectrum D_{tot} defined below eqs. (3.9), (3.10). For cases i) to iii), it is shown in figure 7. Since the maximum of dissipation is in the interior of the wavenumber domain, the simulations are well resolved. The fact that we do not examine higher values of λ, and smaller Fr, in figure 2 is due to this criterion of well-resolvedness. At higher λ, the dissipation spectra showed significant dissipation at the largest $k_\parallel$ and the simulations were thus not well resolved. Therefore, these parameter values were not accessible at the the present resolution. Simulations at higher resolution will be needed to confirm the tentative shape of the phase boundary between forward an inverse cascades at large λ drawn in figure 1.

4.5. *Spatial structures*

Figure 8 shows a visualisation of the density perturbation field ϕ. For case i) there is large-scale organisation in the perpendicular direction, and there is some visible alignment in the parallel direction, in agreement with the 2-D spectra. In case ii), the rotation rate is stronger, leading to a more pronunced alignment in the vertical direction. However, the perpendicular scales in the ϕ field remain small. In case iii), the amplitude of the ϕ field is much higher than in cases i) and ii), and there is a clearly visible large-scale organisation in the parallel

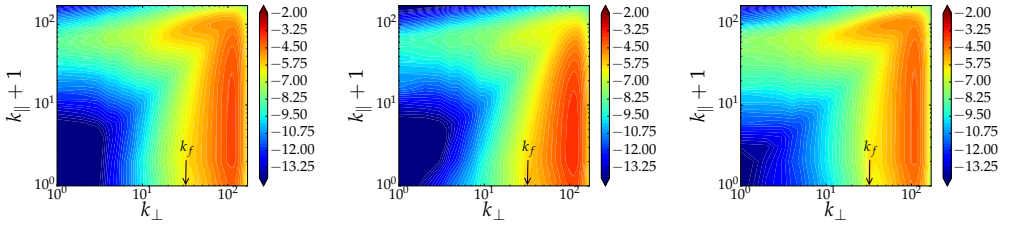

Figure 7: Filled contour plots of 2-D dissipation spectra versus $k_\perp$, $k_\parallel$ for cases i) and iii) (case ii similar). The runs are well resolved since the maximum of dissipation is in the interior of the wavenumber domain.

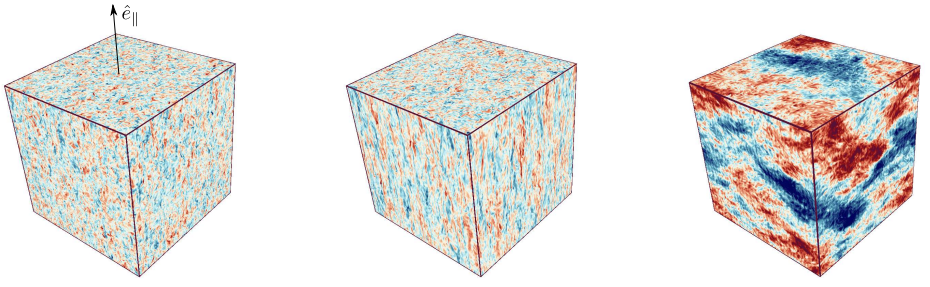

Figure 8: Visualisation of the ϕ field. Left: case i, center: case ii, right: case iii. The black arrow indicates the parallel direction, it is the same for all other visualisations. The colour scale is the same in all three images, with blue colours representing negative values and red colours positive values.

and perpendicular directions. In the parallel direction, there is a layering of density in approximately two layers, which is compatible with the 2-D potential energy spectra. In the perpendicular direction, one can see that the energy is at the largest scale $k_\perp = 1$, since there is one large patch of positive ϕ, and one of negative ϕ (periodic boundaries).
Figure 9 shows a visualisation of the vorticity field. In case i), one sees no large-scale organisation in the perpendicular direction, and there is some rotation-induced alignment along the parallel direction. In case ii), the parallel alignment is more pronounced, since λ is larger, equivalent to faster rotation. In the perpendicular direction, the condensation at the large scales has not yet proceeded far enough to be visible by eye, but 1-D spectrum in figure 3 unequivocally shows that energy is piling up at large scales. Finally, in case iii), there is a clearly visible, high-amplitude pair of counter-rotating vortices on a small-scale background in the perpendicular direction. In the parallel direction, the alignment is weakened by the stronger stratification. We do not show visualisations of the parallel velocity field, since there it features only small-scale structures in all cases.

Figure 10 shows visualisations of the two terms involved in hydrostatic balance (2.12): parallel pressure gradient $2\lambda\partial_\parallel\psi$ and the buoyancy force $-\phi/Fr$. The two fields are visibly highly correlated. Together with the spectra and fluxes above, this validates the proposed explanation of the phenomenology of case iii) based on hydrostatic balance.

5. Discussion

In this paper we investigated energy cascades in stably stratified, rapidly rotating turbulence within an elongated domain. Using a large number of numerical simulations of a reduced system, we constructed a phase diagram of the system, showing that an inverse cascade arises

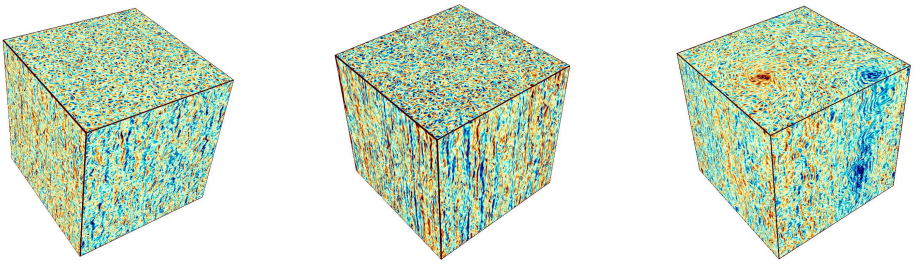

Figure 9: Visualisation of the vorticity field. Left: case i, center: case ii, right: case iii.The colour scale is the same in all three images, with blue colours representing negative values and red colours positive values.

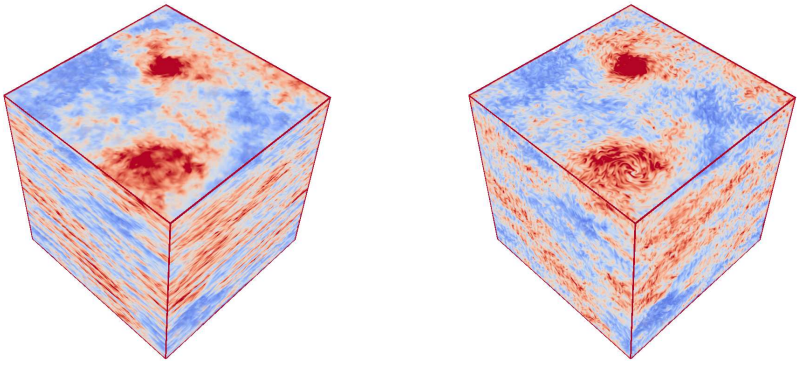

Figure 10: Visualisation of the two terms involved in the hydrostatic balance relation (2.12). Red colours correspond to positive values and blue colours to negative values. The left panel shows $2\lambda\partial_{\|}\psi$, the right panel $-\phi/Fr$. The two fields are clearly correlated.

both for $Fr \gtrsim 1$ and for large $\lambda = (Roh)^{-1}$, while a forward energy cascade is observed for $Fr^{-1} \lesssim 1$ and λ below a threshold λ_c. At strong stratification, we found that approximate hydrostatic balance holds, leading to a non-trivial inverse cascade of both potential and kinetic energy. Future reseach should aim to characterise in more detail the approach to hydrostasy in this extreme parameter regime, in order to better assess its impact on the energy cascades in rotating and stratified turbulence within elongated domains.

Our approach was based on asymptotic reduction, allowing us to reliably achieve the parameter regime of interest at comparatively moderate numerical cost. The asymptotics used here are valid for $Ro \ll 1$, and $Re, Pe, Fr \ll Ro^{-1}$, as well as $Re, Pe, Fr \ll H/\ell_{in}$, while the horizontal box size $L \ll H$. We note in passing that weak wave turbulence is not met in our simulations. This is due to the fact that the tall-box limit and the $Ro \to 0$ limit are taken simultaneously, while weak turbulence requires taking the tall-box limit first (Nazarenko 2011). The efficiency of the procedure is related to the filtering of fast waves by the Taylor-Proudman constraint. It needs to be emphasised, however, that this raises a question about the order of limits. Generally, one is interested in the large-Reynolds-number and large-Peclet-number limits, as well as the limit of large $\Lambda = L/\ell_{in}$. The energy fluxes obtained upon taking these limits first, and then taking $Ro \to 0$ will not, in general, give the same result as when the order is reversed. This calls for investigating also finite values of the parameters using the full rotating and stratified Navier Stokes equations. For the purely rotating problem, (Di Leoni et al. 2020) undertook a step in this direction, showing that meta-stable vortex-crystal states appear near the transition to an inverse cascade, while such

states were not seen in the reduced equations. It is therefore a possibility that the complete phase space of rapidly rotating and stratified turbulence is more complex.

Funding. This work was granted access to the HPC resources of MesoPSL financed by the Region Ile de France and the project Equip@Meso (reference ANR-10-EQPX-29-01) of the programme Investissements d'Avenir supervised by the Agence Nationale pour la Recherche and the HPC resources of GENCI-TGCC & GENCI-CINES (Project No. A0070506421, A0080511423, A0090506421). This work has also been supported by the Agence nationale de la recherche (ANR DYSTURB project No. ANR-17-CE30-0004). AvK acknowledges support by Studienstiftung des deutschen Volkes.

Declaration of interests. Declaration of Interests. The authors report no conflict of interest.

Author ORCID. A. van Kan https://orcid.org/0000-0002-1217-3609; A. Alexakis https://orcid.org/0000-0003-2021-7728

REFERENCES

Alexakis, A. 2011 Two-dimensional behavior of three-dimensional magnetohydrodynamic flow with a strong guiding field. *Phys. Rev. E* **84** (5), 056330.

Alexakis, A. 2015 Rotating taylor–green flow. *J. Fluid Mech.* **769**, 46–78.

Alexakis, Alexandros & Biferale, Luca 2018 Cascades and transitions in turbulent flows. *Physics Reports* **767**, 1–101.

Bartello, Peter 1995 Geostrophic adjustment and inverse cascades in rotating stratified turbulence. *Journal of Atmospheric Sciences* **52** (24), 4410–4428.

Benavides, S. J. & Alexakis, A. 2017 Critical transitions in thin layer turbulence. *J. Fluid Mech.* **822**, 364–385.

Boffetta, G. & Ecke, R. E. 2012 Two-dimensional turbulence. *Ann. Rev. Fluid Mech.* **44** (1), 427–451.

Brethouwer, Geert, Billant, Paul, Lindborg, Erik & Chomaz, J-M 2007 Scaling analysis and simulation of strongly stratified turbulent flows. *Journal of Fluid Mechanics* **585**, 343–368.

Calkins, Michael A, Julien, Keith, Tobias, Steven M & Aurnou, Jonathan M 2015 A multiscale dynamo model driven by quasi-geostrophic convection. *Journal of Fluid Mechanics* **780**, 143–166.

Celani, Antonio, Cencini, Massimo, Mazzino, Andrea & Vergassola, Massimo 2004 Active and passive fields face to face. *New Journal of Physics* **6** (1), 72.

Celani, A., Musacchio, S. & Vincenzi, D. 2010 Turbulence in more than two and less than three dimensions. *Phys. Rev. Lett.* **104**, 184506.

Davidson, Peter Alan 2013 Turbulence in rotating, stratified and electrically conducting fluids. Cambridge University Press.

Deusebio, E., Boffetta, G., Lindborg, E. & Musacchio, S. 2014 Dimensional transition in rotating turbulence. *Phys. Rev. E* **90** (2), 023005.

Di Leoni, P Clark, Alexakis, Alexandros, Biferale, L & Buzzicotti, M 2020 Phase transitions and flux-loop metastable states in rotating turbulence. *Physical Review Fluids* **5** (10), 104603.

Ertel, Hans 1942 Ein neuer hydrodynamischer erhaltungssatz. *Naturwissenschaften* **30** (36), 543–544.

Falkovich, Gregory, Gawedzki, K & Vergassola, Massimo 2001 Particles and fields in fluid turbulence. *Reviews of modern Physics* **73** (4), 913.

Favier, B., Silvers, L. J. & Proctor, M. R. E. 2014 Inverse cascade and symmetry breaking in rapidly rotating boussinesq convection. *Phys. Fluids* **26** (9), 096605.

Fjørtoft, Ragnar 1953 On the changes in the spectral distribution of kinetic energy for twodimensional, nondivergent flow. *Tellus* **5** (3), 225–230.

Frisch, U. 1995 Turbulence: the legacy of AN Kolmogorov. Cambridge University Press.

Gibson, Carl H 1991 Laboratory, numerical, and oceanic fossil turbulence in rotating and stratified flows. *Journal of Geophysical Research: Oceans* **96** (C7), 12549–12566.

Greenspan, Harvey Philip Greenspan & others 1968 The theory of rotating fluids. CUP Archive.

Grooms, Ian, Julien, Keith, Weiss, Jeffrey B & Knobloch, Edgar 2010 Model of convective taylor columns in rotating rayleigh-bénard convection. *Physical review letters* **104** (22), 224501.

Guervilly, Céline & Hughes, David W 2017 Jets and large-scale vortices in rotating rayleigh-benard convection. *Physical Review Fluids* **2** (11), 113503.

Guervilly, C., Hughes, D. W. & Jones, C. A. 2014 Large-scale vortices in rapidly rotating rayleigh–bénard convection. *J. Fluid Mech.* **758**, 407–435.

Herbert, Corentin, Pouquet, Annick & Marino, Raffaele 2014 Restricted equilibrium and the energy cascade in rotating and stratified flows. *arXiv preprint arXiv:1401.2103* .

Herring, Jackson R & Métais, Olivier 1989 Numerical experiments in forced stably stratified turbulence. *Journal of Fluid Mechanics* **202**, 97–115.

Hoskins, BJ, Draghici, I & Davies, HC 1978 A new look at the ω-equation. *Quarterly Journal of the Royal Meteorological Society* **104** (439), 31–38.

Hoskins, Brian, Pedder, Mike & Jones, David Wyn 2003 The omega equation and potential vorticity. *Quarterly Journal of the Royal Meteorological Society* **129** (595), 3277–3303.

Hough, Sydney Samuel 1897 Ix. on the application of harmonic analysis to the dynamical theory of the tides.—part i. on laplace's "oscillations of the first species" and the dynamics of ocean currents. *Philosophical Transactions of the Royal Society of London. Series A, Containing Papers of a Mathematical or Physical Character* (189), 201–257.

Julien, Keith, Knobloch, Edgar, Milliff, Ralph & Werne, Joseph 2006 Generalized quasi-geostrophy for spatially anisotropic rotationally constrained flows. *Journal of Fluid Mechanics* **555**, 233–274.

Julien, Keith, Knobloch, Edgar & Plumley, Meredith 2018 Impact of domain anisotropy on the inverse cascade in geostrophic turbulent convection. *Journal of Fluid Mechanics* **837**.

Julien, Keith, Knobloch, Edgar, Rubio, Antonio M & Vasil, Geoffrey M 2012a Heat transport in low-rossby-number rayleigh-bénard convection. *Physical review letters* **109** (25), 254503.

Julien, Keith, Knobloch, Edgar & Werne, Joseph 1998 A new class of equations for rotationally constrained flows. *Theoretical and computational fluid dynamics* **11** (3-4), 251–261.

Julien, K, Rubio, AM, Grooms, I & Knobloch, E 2012b Statistical and physical balances in low rossby number rayleigh–bénard convection. *Geophysical & Astrophysical Fluid Dynamics* **106** (4-5), 392–428.

van Kan, Adrian & Alexakis, Alexandros 2019 Condensates in thin-layer turbulence. *Journal of Fluid Mechanics* **864**, 490–518.

van Kan, Adrian & Alexakis, Alexandros 2020 Critical transition in fast-rotating turbulence within highly elongated domains. *Journal of Fluid Mechanics* **899**.

van Kan, Adrian, Nemoto, Takahiro & Alexakis, Alexandros 2019 Rare transitions to thin-layer turbulent condensates. *Journal of Fluid Mechanics* **878**, 356–369.

Kurien, S, Wingate, B & Taylor, MA 2008 Anisotropic constraints on energy distribution in rotating and stratified turbulence. *EPL (Europhysics Letters)* **84** (2), 24003.

Leith, CE 1980 Nonlinear normal mode initialization and quasi-geostrophic theory. *Journal of Atmospheric Sciences* **37** (5), 958–968.

Maffei, S, Krouss, MJ, Julien, K & Calkins, MA 2021 On the inverse cascade and flow speed scaling behaviour in rapidly rotating rayleigh–benard convection. *Journal of Fluid Mechanics* **913**.

Marino, Raffaele, Mininni, Pablo Daniel, Rosenberg, Duane & Pouquet, Annick 2013 Inverse cascades in rotating stratified turbulence: fast growth of large scales. *EPL (Europhysics Letters)* **102** (4), 44006.

Marino, Raffaele, Mininni, Pablo Daniel, Rosenberg, Duane L & Pouquet, Annick 2014 Large-scale anisotropy in stably stratified rotating flows. *Physical Review E* **90** (2), 023018.

Marino, R., Pouquet, A. & Rosenberg, D. 2015 Resolving the paradox of oceanic large-scale balance and small-scale mixing. *Phys. Rev. Lett.* **114** (11), 114504.

Maxworthy, T & Browand, FK 1975 Experiments in rotating and stratified flows: oceanographic application. *Annual Review of Fluid Mechanics* **7** (1), 273–305.

Mininni, P. D., Rosenberg, D., Reddy, R. & Pouquet, A. 2011 A hybrid mpi–openmp scheme for scalable parallel pseudospectral computations for fluid turbulence. *Parallel Computing* **37** (6-7), 316–326.

Musacchio, S. & Boffetta, G. 2017 Split energy cascade in turbulent thin fluid layers. *Phys. Fluids* **29** (11), 111106.

Musacchio, Stefano & Boffetta, Guido 2019 Condensate in quasi-two-dimensional turbulence. *Physical Review Fluids* **4** (2), 022602.

Nazarenko, Sergey 2011 Wave turbulence, , vol. 825. Springer Science & Business Media.

Nazarenko, Sergei V & Schekochihin, Alexander A 2011 Critical balance in magnetohydrodynamic, rotating and stratified turbulence: towards a universal scaling conjecture. *Journal of Fluid Mechanics* **677**, 134–153.

Oks, D, Mininni, Pablo Daniel, Marino, Raffaele & Pouquet, Annick 2017 Inverse cascades and resonant triads in rotating and stratified turbulence. *Physics of Fluids* **29** (11), 111109.

Pedlosky, J. 2013 Geophysical fluid dynamics. Springer Science & Business Media.

Pestana, Tiago & Hickel, Stefan 2019 Regime transition in the energy cascade of rotating turbulence. *Physical Review E* **99** (5), 053103.

Poujol, Basile, van Kan, Adrian & Alexakis, Alexandros 2020 Role of the forcing dimensionality in thin-layer turbulent energy cascades. *Physical Review Fluids* **5** (6), 064610.

Pouquet, Annick, Marino, Raffaele, Mininni, Pablo Daniel & Rosenberg, Duane 2017 Dual constant-flux energy cascades to both large scales and small scales. *Physics of Fluids* **29** (11), 111108.

Pouquet, A, Rosenberg, D, Stawarz, JE & Marino, R 2019 Helicity dynamics, inverse, and bidirectional cascades in fluid and magnetohydrodynamic turbulence: a brief review. *Earth and Space Science* **6** (3), 351–369.

Proudman, Joseph 1916 On the motion of solids in a liquid possessing vorticity. *Proceedings of the Royal Society of London. Series A, Containing Papers of a Mathematical and Physical Character* **92** (642), 408–424.

Rosenberg, Duane, Pouquet, Annick, Marino, Raffaele & Mininni, Pablo Daniel 2015 Evidence for bolgiano-obukhov scaling in rotating stratified turbulence using high-resolution direct numerical simulations. *Physics of Fluids* **27** (5), 055105.

Rubio, A. M., Julien, K., Knobloch, E. & Weiss, J. B. 2014 Upscale energy transfer in three-dimensional rapidly rotating turbulent convection. *Phys. Rev. Lett.* **112** (14), 144501.

Sahoo, G., Alexakis, A. & Biferale, L. 2017 Discontinuous transition from direct to inverse cascade in three-dimensional turbulence. *Phys. Rev. Lett.* **118** (16), 164501.

Sahoo, G. & Biferale, L. 2015 Disentangling the triadic interactions in navier-stokes equations. *Eur. Phys. J. E* **38** (10), 114.

Salmon, Rick 1998 Lectures on geophysical fluid dynamics. Oxford University Press.

Seshasayanan, K. & Alexakis, A. 2016 Critical behavior in the inverse to forward energy transition in two-dimensional magnetohydrodynamic flow. *Phys. Rev. E* **93** (1), 013104.

Seshasayanan, K. & Alexakis, A. 2018 Condensates in rotating turbulent flows. *J. Fluid Mech.* **841**, 434–462.

Seshasayanan, K., Benavides, S. J. & Alexakis, A. 2014 On the edge of an inverse cascade. *Phys. Rev. E* **90** (5), 051003.

Smith, L. M., Chasnov, J. R. & Waleffe, F. 1996 Crossover from two-to three-dimensional turbulence. *Phys. Rev. Lett.* **77** (12), 2467.

Smith, Leslie M & Waleffe, Fabian 2002 Generation of slow large scales in forced rotating stratified turbulence. *Journal of Fluid Mechanics* **451** (1), 145–168.

Sozza, A., Boffetta, G., Muratore-Ginanneschi, P. & Musacchio, S. 2015 Dimensional transition of energy cascades in stably stratified forced thin fluid layers. *Phys. Fluids* **27** (3), 035112.

Sprague, Michael, Julien, Keith, Knobloch, Edgar & Werne, Joseph 2006 Numerical simulation of an asymptotically reduced system for rotationally constrained convection. *Journal of Fluid Mechanics* **551**, 141–174.

Sukhatme, Jai & Smith, Leslie M 2008 Vortical and wave modes in 3d rotating stratified flows: random large-scale forcing. *Geophysical and Astrophysical Fluid Dynamics* **102** (5), 437–455.

Taylor, Geoffrey Ingram 1917 Motion of solids in fluids when the flow is not irrotational. *Proceedings of the Royal Society of London. Series A, Containing Papers of a Mathematical and Physical Character* **93** (648), 99–113.

Thomas, Jim & Daniel, Don 2021 Forward flux and enhanced dissipation of geostrophic balanced energy. *Journal of Fluid Mechanics* **911**.

Trustrum, Kathleen 1964 Rotating and stratified fluid flow. *Journal of Fluid Mechanics* **19** (3), 415–432.

Vallis, Geoffrey K 2017 Atmospheric and oceanic fluid dynamics. Cambridge University Press.

Waite, Michael L & Bartello, Peter 2004 Stratified turbulence dominated by vortical motion. *Journal of Fluid Mechanics* **517**, 281.

Warhaft, Zellman 2000 Passive scalars in turbulent flows. *Annual Review of Fluid Mechanics* **32** (1), 203–240.

Yokoyama, N. & Takaoka, M. 2017 Hysteretic transitions between quasi-two-dimensional flow and three-dimensional flow in forced rotating turbulence. *Phys. Rev. Fluids* **2** (9), 092602.